QUANTITATIVE INFRARED THERMOGRAPHY JOURNAL
https://doi.org/10.1080/17686733.2024.2448049

Taylor & Francis
Taylor & Francis Group

REVIEW ARTICLE

OPEN ACCESS Check for updates

Inductive thermography – review of a non-destructive inspection technique for surface crack detection

Beate Oswald-Tranta

Chair of Automation and Measurement, University of Leoben, Leoben, Austria

ABSTRACT

Inductive thermography is an excellent inspection technique for detecting defects in metallic materials. The technique has been greatly improved over the last few decades, from laboratory experiments to industrial applications. Many researches have studied the theory and the physical processes behind inductive thermography and also how the experimental setup and the evaluation of the results can be improved. The purpose of this paper is to give an overview of the theory and also of the most important technical points which should be taken into consideration for the usage of this technique. However, if inductive thermography can be used to locate various types of defects, this paper focuses on the detection of surface cracks in metals. In addition, several examples are given of how this inspection technique is used nowadays in industrial applications.

ARTICLE HISTORY
Received 23 October 2024
Accepted 24 December 2024

KEYWORDS
Inductive thermography; crack detection; crack characterisation

1. Introduction

In the case of inductive thermography, a short inductive heating pulse is applied to the work-piece to be inspected and an infrared (IR) camera records its surface temperature. Due to the material's ohmic resistance, Joule heat is generated in the work-piece. Defects, such as cracks, affect both the eddy current distribution and the heat flow, making the defects visible in the IR images [1].

The technique can be used for inspecting electrically conductive materials. In most of the cases, it is used for testing metals. However, since carbon fibres conduct electricity, CFRP structures can also be inspected by using inductive thermography. Several research groups have inspected CFRP structures, and reported that fibre breaks caused by impact damages can be excellently detected by inductive thermography [2–6]. Additionally, as the electrical current is flowing along the carbon fibres, the method gives a possibility to inspect the fibre orientation [7].

Inductive thermography is very sensitive to detecting surface cracks, but there are also other situations where the technique can be excellently used, e.g. to inspect welding, whether two metal plates are really connected by the weld or not. Another possibility is to detect subsurface defects by inductive thermography. In this case, similarly to optically

CONTACT Beate Oswald-Tranta beate.oswald@unileoben.ac.at Chair of Automation and Measurement, University of Leoben, Peter-Tunnerstr.27, Leoben 8700, Austria

excited thermography, the heat generated close to the surface flows into the material and will be disturbed or reflected by subsurface defects. This perturbation inside the material can be observed at the surface temperature, which reveals the subsurface defects. Several papers are published, comparing detection of subsurface defects using inductive or optically induced thermography, as e.g. in Refs [8,9].

However, this paper focuses on the usage of inductive thermography to detect surface cracks in metals. The induced eddy currents flow in a region below the surface, in the so-called skin depth. As surface cracks are obstacles for the eddy current flow, the currents flow around the crack, causing a selective heating of the defects. How deep this skin-depth is, affected by many factors, as by the material parameters, but also by the excitation frequency. Several research groups have investigated the effect of these factors on the Joule heating, which can be produced in different metals [10,11]. For the modelling of the eddy current flow around cracks multi-physics FEM simulations are necessary, which are able to model electromagnetic and the thermal process together [12–14]. These simulations help to understand the processes of inductive heating, but they also help to optimise the inspection technique and leading further from laboratory experiments up to industrial applications.

This paper is organised in the following way: after a short overview of the physics behind the induction thermography, several technical aspects of the setup are discussed. The evaluation of the recorded IR sequence and its combination with other techniques are then summarised. In the recent years, several approaches have been developed to fully automate the inspection, both in terms of specimen handling and defect location and the characterisation. These results lead to industrial applications, some of which are described in the last section of the paper.

2. Eddy current flow around surface cracks

An alternating voltage is induced in a work-piece, when it is placed in an alternating magnetic field. In an electrically conductive material, this further induces an electrical current, known as eddy current. The induced eddy current decays exponentially below the surface, and it penetrates only into a thin skin, which is characterised by the penetration depth or skin depth:

$$\delta = \sqrt{\frac{1}{\pi \mu_0 \mu_r \sigma f}}, \tag{1}$$

where μ_0 is the vacuum permeability with the value of $4\pi 10^{-7}$ Vs/Am; μ_r is the relative magnetic permeability of the material; σ is its electrical conductivity and f is the excitation frequency. For austenitic steel, which is non-magnetic, the skin depth is approximately 1.34 mm, at an excitation frequency of $f = 100$ kHz. For a typical ferro-magnetic steel, due to its magnetic property of $\mu_r = 600$, the penetration depth is only 0.048 mm for the same excitation frequency. Table 1 summarises for the inductive thermography relevant material parameters for these two materials. The value of the skin depth has a strong influence on the results of an inductive thermography measurement, especially by comparing this value to the depth of the surface crack, which should be detected.

Table 1. Material parameters.

Material	Electrical conductivity σ [Ω^{-1} $^{-1}$m^{-1}]	Relative permeability μ_r [-]	Thermal conductivity λ [W m^{-1}K^{-1}]	Specific heat capacity c [J kg^{-1} K^{-1}]	Thermal diffusivity K [m^2 s^{-1}]	Penetration depth if f=100kHz [mm]
Steel ferro-magn.	1.85 x 10^6	600	40	410	1.16 x 10^{-5}	0.048
Steel AISI304 non-magn.	1.39 x 10^6	1	16	500	4 x 10^{-6}	1.34

The exponential decay function is strictly valid only for a semi-infinite long plane surface. For other geometries, such as the case around a surface crack, the eddy currents flow around the obstacle. To calculate the eddy current, the Joule heating and the temperature distribution for this situation, finite element simulations can be used. ANSYS multi-physics package is **κ** possible choice for such FEM calculations, as it is able to couple the electromagnetic and the thermal processes in the modelling. The simulation results show that the current does not exactly follow the side of the work-piece, as e.g. in the case of a corner the current flow is pushed away from the corner at a distance of about twice the penetration depth [14], see Figure 1a. Due to the ohmic resistance of the material, along the eddy current flow Joule heating is generated, which furthermore results in inhomogeneous heating around the defects. The inhomogeneous Joule heating causes an inhomogeneous temperature distribution at the surface, see Figure 1c,d, showing the temperature distribution at the end of a 100 ms inductive heating pulse. This inhomogeneous surface temperature distribution can be recorded by an infrared camera and used for localising the defects. It is to emphasise that defects disturb the eddy current flow as well as the heat diffusion, therefore the temperature difference caused by

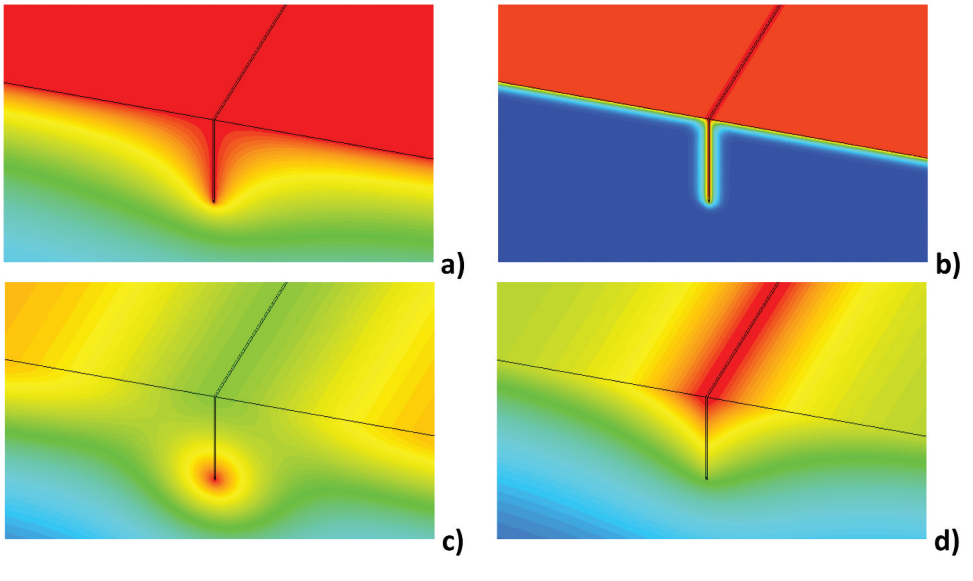

Figure 1. Simulation results for a 1 mm deep crack: eddy current distribution in non-magnetic AISI steel (a) and in ferro-magnetic steel (b) by 100 kHz excitation frequency; temperature distribution after 100 ms heating pulse in non-magnetic AISI steel (c) and in ferro-magnetic steel (d).

a crack is much larger than in the case, e.g. by laser heating, where only the lateral heat flow is disturbed by a defect, but not the heating process itself.

For ferro-magnetic materials, the penetration depth is very small ($\delta = 0.048$ mm) compared to the depth of a surface crack, which usually should be detected ($d = 0.5$–1 mm). With a good estimation, the inductive heating can be modelled as a surface heating that also occurs along the crack sides in the material, see Figure 1b. The assumption of a surface heating allows even an analytical modelling of the inductive thermography, as it has been shown in Ref [15]. Due to the heat accumulation in the corners of a surface cracks, in ferro magnetic materials a crack can be detected due to higher temperature at the surface (see Figure 1d).

On the other hand, in non-magnetic materials, where the eddy current penetration depth is comparable or greater than the typical surface crack depth, it has the significant effect that the eddy current at the corner of the crack flows in a distance from the surface. As the current flow is pushed away from the crack, there is locally less Joule heating around the crack at the surface, therefore the crack can be detected by observing lower temperature values at the surface, see Figure 1a and c.

The deeper a crack is, the greater the obstacle it represents for the eddy currents and also for the heat diffusion. Therefore, the temperature perturbation in the vicinity of a crack is significantly related to its depth. This is one of the main advantages of the inductive thermography: the measured signal strength can be used to estimate the depth of the crack below the surface [14].

The previous statements treated a crack as a long crack, without considering the effects around the crack tip at the surface. Figure 2a shows the temperature around a 3-mm-long surface crack in a non-magnetic austenitic steel specimen. In the central part of the crack, the eddy current flows below the surface, resulting in a lower temperature value than at the defect-free surface, in a similar way as is the case for a long crack. However, around the crack tip there is a higher current density, resulting in a high temperature hot spot.

The inclination angle of the crack also affects the eddy current as well as the heat diffusion. The cracks discussed previously, penetrated perpendicularly to the surface into

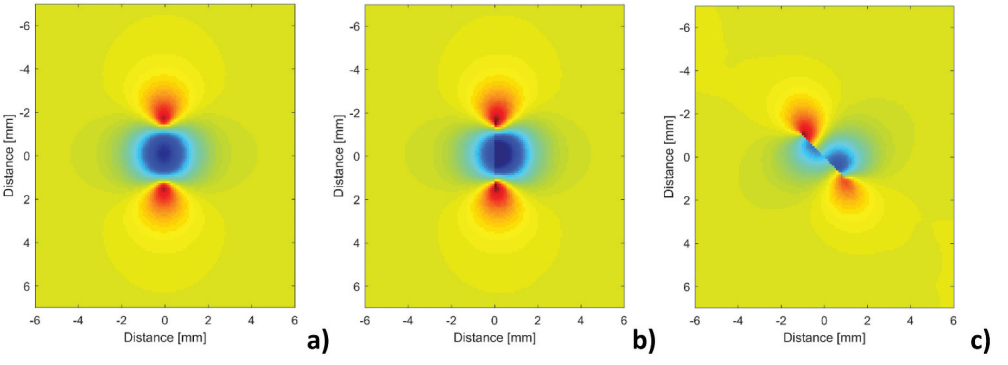

Figure 2. Simulated temperature results for a 3 mm long and 1 mm deep crack after 100 ms inductive heating pulse: crack is perpendicular to the surface and to the eddy current direction (a); crack has an inclination angle of 30° and perpendicular to the eddy current direction (b) and having 45° to the eddy current direction (c).

the material. If the crack is inclined, then the observed temperature pattern on the both sides of the crack becomes asymmetrical [16], see Figure 2b.

When the induced eddy current hits the crack at 90°, the disturbance caused by the crack is the greatest. This case has been demonstrated in the previous figures. If the angle between the crack line and the eddy currents is less than 90°, then the pattern is rotated [16], see Figure 2c. However, if the eddy currents flow parallel to the crack line, then the crack is no longer an obstacle to the current and no temperature perturbation due to the crack can be observed. This type of problem is well known from magnetic particle testing, where if the magnetisation is parallel to the crack line, then the crack cannot be detected.

In the inductive thermography inspection, the sample is heated usually just 1–2 degrees, therefore the temperature dependency of the material parameters can be neglected. This further means that all the equations are linear equations and doubling the induced heat amount doubles the temperature increase. In such way, the simulated temperature distributions in Figures 1 and 2 can be taken as values in arbitrary units, their real value will be only then relevant, if they are compared to measurement noise.

3. Experimental setup

3.1 Induction generator

The two main hardware components required for inductive thermography inspection are an infrared camera and an induction generator with an inductor. There are two types of generators commonly used: one with a water-cooled copper coil and one with an air-cooled ferrite core inductor, see Figure 3. The first type of generator operates as a resonant circuit. Internal capacitors and the external copper coil together with the sample form a resonant circuit, and the excitation frequency of the generator is close to this resonance frequency. This type of generator can provide large induction power, even up to 20 kW is possible. On the other hand, the copper coil carries a large electrical current and therefore usually needs to be water cooled. The induction coil is made of a copper tube with water cooling inside. This generator is able to produce magnetic field in a large

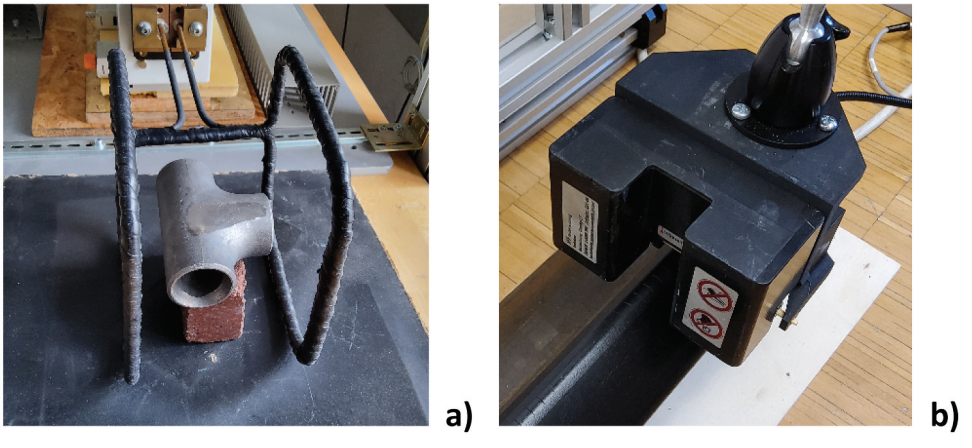

Figure 3. Two types of inductors: water-cooled Helmholtz coil (a); air-cooled ferrite-core inductor (b).

space, therefore, e.g. a work-piece can be placed inside the coil. Figure 3a shows a so-called Helmholtz coil, which has the advantage, that the magnetic field between the two windings is almost homogeneous and it also allows the IR camera's view to inspected surface [17].

In other cases, when the work-piece to be inspected is large, then other coil geometries have to be selected, which are placed above the surface. Figure 4 shows other frequently used coil geometries. Generally, the induced eddy currents 'mirror' the geometry of the induction coil, so in the case of a circular coil the induced eddy currents flow in a circular form (see Figure 4a). This causes an inhomogeneous heating, close to the coil the heating is much larger than in the middle of the circle, which can furthermore cause inhomogeneity in the detectability of defects. The induction coil may consist of more windings above each other, see Figure 4b or around each other, see Figure 4c. The number of the windings multiply the induced magnetic heat flux and the Joule heating increases with the squares of the number of turns. On the other hand, the number of turns increases the inductivity of the coil, which can reduce the electrical current, which is maximal deliverable by the generator. The optimal number of windings and the size of the coil depends on the application itself and the specifications of the generator.

This type of generator has the disadvantage, that the excitation frequency cannot be easily changed; additional capacitors can be added or the geometry of the copper induction coil can be modified, but with these settings the output working frequency is fixed. The usual working frequency range of this type of generators is between 40 kHz and 200 kHz.

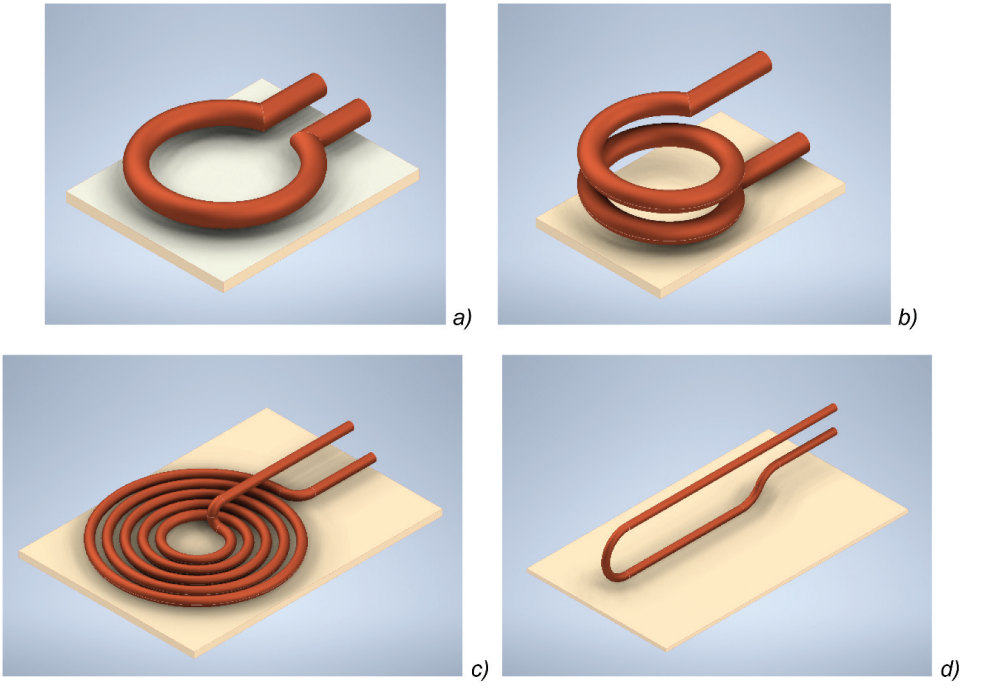

Figure 4. Different coil types: circular coil (a); circular coil with more windings (b); pancake coil (c); linear coil (d).

The second type of generator uses hard-chopper technique with insulated-gate bipolar transistors (IGBTs) and pulse width modulation [18]. For the inductor copper wires are wrapped around a ferrite core, which normally does not need to be cooled. The output frequency can be set by software via control parameters, e.g. in a range between 25 kHz and 60 kHz. The spatial area of the excitation is small, determined by the size of the ferrite core, see Figure 3b. However, this type of generator has the advantage of being easy to use, as no water cooling is required. Table 2 compares the most important characteristics of these two generator types.

The induction coils of Figure 4 and the ferrite-core inductor, shown in Figure 3b, are placed above the surface. With increasing distance between the inductor and the surface the induced heat amount is reduced. This problem is well known from the eddy current testing, and it is called the 'lift-off' effect. Usually, a couple of mm distance is kept between the inductor and the surface, in order to generate enough heating, but do not touch the surface. This problem does not occur in the case of the Helmholtz coil, as it is also shown in Figure 3a. There is enough space between the work-piece and the induction coil even during the measurement, e.g. a robotic arm can hold the work-piece [19].

Both of these generators are large and not appropriate for portable applications. The authors of Ref [20] report experiments with a small, low-cost, portable ZVS (Zero voltage switching) heat source, which could provide a new possibility for inductive thermography in in-field inspections.

As mentioned above, the detectability of the crack depends on the angle between the orientation of the induced magnetic field and the crack. In a general setup, in order to detect any crack orientation, two measurements are required, with two different magnetic field orientations at 90° to each other. There have been several suggestions how the measurement can be made without physically rotating the inductor. In the case of water-cooled Helmholtz coil setup, it is possible to use two such kind of coils placed 90° to each other and applying slightly different excitation frequencies, as it is suggested in Ref [17]. In this way, the magnetic field rotates, describing Lissajous curves, and any crack orientations can be detected.

For the generators with ferrite core inductor, it is possible to design the ferrite cores in such a way that there are separate ferrite cores with copper windings included in one inductor, and they are responsible to generate the magnetic field in different directions. The different windings on the different ferrite cores are then electrically switched on one after the other. In this way, no movement of the inductor is required, and the different magnetic field orientations are measured after each other [21–23].

Table 2. Comparison of the two different types of generators.

Generator as resonant circuit	Generator with hard-chopper technique
High frequency (HF), up to 450 kHz	Mid frequency (MF), 20–60 kHz
Working frequency can be changed by mounting additional capacitors into the generator	Working frequency can be changed via software interface
Induction coil: copper tube	Ferrite core with copper windings
For generator and induction coil water cooling is necessary	Usually air cooling is enough
Spatial area of inspection – scalable up to large sizes (e.g. 400 x 400 mm^2)	Spatial area is small, determined by the ferrite core (e.g. 30 x 30 mm^2)
Pulse or continuous heating	Only pulse heating is possible

Both types of generator can be used in a static or in a scanning mode. In static mode, none of the components moves and the IR camera records the surface temperature during the heating pulse. In many cases, it has been found advantageous to record the surface temperature not only during the heating pulse but also afterwards, during the cool-down phase. The whole recorded IR sequence, i.e. the temporal change of the temperature for each pixel, is then analysed. Usually, a short inductive pulse, between 50 ms and 1 s, is applied. The shorter the pulse, the sharper the contrast as there is less time for the temperature difference to equalise due to heat diffusion. On the other hand, a shorter heating pulse means less induced energy, which in turn means less signal and therefore a lower signal-to-noise ratio. The optimum choice of the heating pulse length is an important factor, determined by the experimental setup and by the defects to be detected.

In the case of scanning mode, there is a relative movement between the inspected sample and the inductor [24]. The IR camera remains fixed to the excitation. This type of method is used, when inspecting long pieces such as semi-finished products, as steel billet or rails. For the scanning technique, the same inductors can be used, as for the static inspection. But the line inductor, shown in Figure 4d, is a very useful choice, for scanning the surface through with an approximate line heating, which is well comparable to an instantaneous surface heating [25]. As the camera records the temperature from a different area of the specimen due to the movement, either the temperature images themselves are analysed or the recorded sequence has to be reordered to obtain a quasi-static IR sequence, see later on in Section 4.

3.2 Infrared camera for inductive thermography

There are two types of infrared cameras, which are used in thermographic inspections: microbolometer and photonic detectors [26]. Microbolometers are thermal detectors, which means, the infrared radiation is absorbed by the detector element (microbolometer pixel) and its electrical conductivity changes with the temperature, which is then measured by reading out the information from the pixels. Photonic detectors consist of semiconductor materials, where the energy of the photons of the infrared radiation has to have the energy corresponding to the energy gap of the semiconductor. The absorbed photon energy generates additional charge carriers, electrons and holes, and generates a photo current in the photo diode, i.e. in each pixel of the IR camera. There are further new developments in semiconductor detectors, which do not include p-n photo diodes, as e.g. QWIP and superlattice structures. A detailed description of all kind of infrared detectors can be found in Ref [26].

To decide what kind of IR camera should be used for a thermographic inspection application, the three different resolutions of an IR camera should be investigated more closely for the given task:

- Temporal resolution: with which frequency the IR camera can record the images;
- Thermal resolution: it can be characterised by the NETD (Noise Equivalent Temperature Difference)

- Spatial resolution: on to how many pixels one mm of the object is mapped. This is determined by the optic of the camera, by the number of the pixels of the camera and by the distance between camera and the object.

Table 3 compares the most important properties of these two camera types. Microbolometer cameras are much cheaper than photonic cameras, and as they do not need a cooling, they are more suitable for inspection in industrial environment. On the other hand, they have much lower resolutions, which are for many inspection applications not sufficient and therefore a photonic IR camera has to be used.

Photonic detectors work in snapshot mode, which means that all the pixels are read out at the same time. On the other hand, microbolometer cameras read out continuously the pixels of one image. In such way, the pixels of one image represent the temperature in slightly different time. This characteristic can be important by scanning measurements. Due to the different read-out time, the object moves further during recording of one image and the pixels show the object in different positions, which may cause a distorted image [27]. Additionally, microbolometer cameras have a time constant of around 8–10 ms, which means this is the time needed for recording one image. As during this time, the object moves further, this may cause a motion blurring of the recorded IR image. If the object's motion speed and the spatial resolution are known, then this motion blurring can be well eliminated and the image reconstructed by image processing techniques [27].

4. Evaluation of the infrared images

In the case of static measurement, the temporal change in temperature is recorded during the heating pulse and also during the cooling time. If only one single temperature image at the end of the heating pulse is evaluated, it will be affected by negative effects, such as inhomogeneous heating and inhomogeneous emissivity of the surface. The most practicable way to reduce these negative effects is to use the PPT technique [28] and calculate a phase value for each pixel by applying the Fourier transform:

$$F_\tau = \int_0^\tau T(t) e^{\frac{-i2\pi t}{\tau}} dt \tag{2}$$

$$\varphi = \arctan \frac{\mathrm{Im}(F_\tau)}{\mathrm{Re}(F_\tau)} \tag{3}$$

where $\tau = t_{pulse} + t_{cooldown}$. The duration of $t_{cooldown}$ is usually chosen to be equal to t_{pulse}. Note, that since the recorded IR sequence is not continuous, the Fourier transform is

Table 3. Most important properties of two kinds of IR camera types.

	Microbolometer	Photonic detector
NETD	50–80 mK	<20 mK
Recording frequency	8–50 hz	200–2000 hz
Working temperature	Uncooled, room temperature	Cooled, < 80 K
Usual spectral range	8–14 µm	1.5–5 µm
Read-out	Continuous read-out of the pixels	Snapshot mode

calculated by using the Discrete Fourier Transform (DFT). Due to the normalisation of the phase calculation, the above mentioned inhomogeneity effects are strongly reduced [29].

Originally, the PPT technique has been developed to detect subsurface defects by applying optical heating with a flash lamp. In the case of subsurface defects, the thermal waves are reflected from different depths of the defects. Therefore, several frequencies of the Fourier transform spectrum are analysed, as their behaviour gives information about how deep the defect is below the surface. In the case of surface crack detection using inductive thermography, the physical meaning of the phase values is different. It does not represent the phase shift of the thermal waves due to reflection from the depth, but rather it shows, how fast or slow the heating and cooling occurs at each pixel location [29].

As mentioned in the previous section, shorter heating pulses produce sharper images because there is less time for the heat diffusion. But the short heating pulse delivers less energy, which can lead to noisy images, especially for non-magnetic materials, where the inductive heating is less efficient. Figure 5 demonstrates this situation: Figure 5a is measured with a 50 ms heating pulse, which means less energy, less heating applied to the sample, than in the case of Figure 5b, with 100 ms heating pulse. Therefore, Figure 5a is more noisy. On the other hand, as shallower cracks cause less perturbation, with a longer measurement time the heat diffusion can blur the image, and shallower cracks could be missed.

Similar to the lock-in technique developed to detect subsurface defects by applying sinusoidal thermal heating over several periods [30–34], this technique can also be adapted to inductive thermography [35,36]. Several heating pulses are applied in succession, and the phase value is calculated for the frequency of $f = 1/\tau$:

$$F_{n,N_{pulse}} = \frac{2}{n \cdot N_{pulse}} \cdot \sum_{j=1}^{N_{pulse}} \sum_{k=0}^{n} T_k \, e^{-2\pi k i/n} \tag{4}$$

where n is the number of images recorded during one period and N_{pulse} is the number of pulses recorded. It can be shown that this calculation reduces the noise by $\sqrt{n \cdot N_{pulse}}$, i.e.

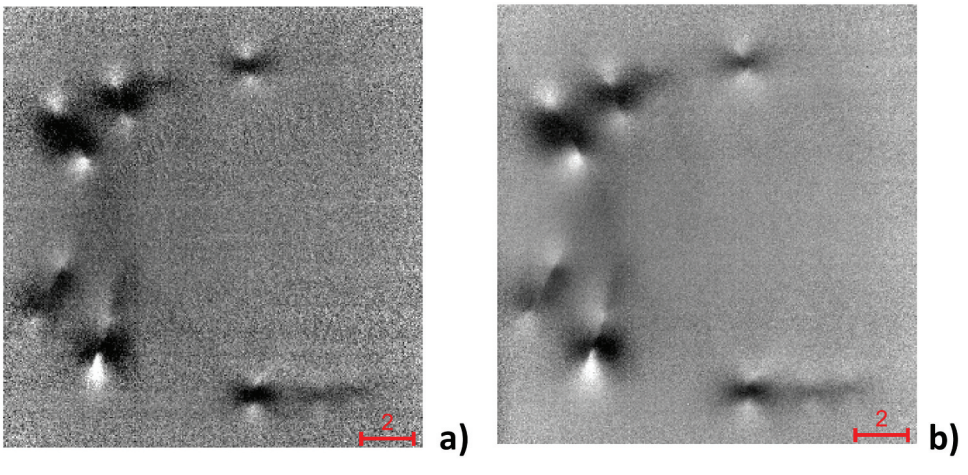

Figure 5. Phase image of a weld with small surface cracks after a heating pulse with 50 ms (a) and after a heating pulse with 100 ms (b).

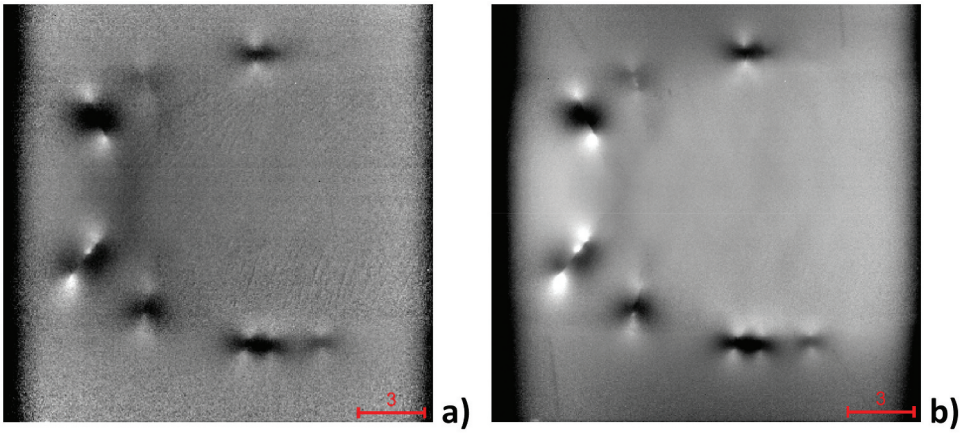

Figure 6. Phase image of a weld with small surface cracks after one heating pulse (a) and after 10 pulses (b).

the higher the IR camera's recording frame rate and the more pulses are recorded, the better the noise reduction [34,36]. Figure 6 illustrates this effect for another weld sample: 10 consecutive heating pulses, each of them with 100 ms duration, were applied to the sample. After each heating pulse an additional 100 ms is recorded during the cooling time. Figure 6a shows the phase image, evaluated for the first heating pulse only. In Figure 6b all the ten heating pulses are evaluated, for the frequency of $f = 1/(2 \times 100\ \text{ms}) = 5$ Hz. It can be observed, that the noise is strongly reduced by evaluating ten pulses, and so the cracks become clearer detectable.

In the case of scanning measurements, the IR camera records the temperature during the motion of the object. Figure 7a shows such an IR image: on the left side a linear induction coil is visible and the object moves from the left side to the right, heated inductively. Extracting from the whole IR sequence one column of pixels, one IR image of the object in a specified distance from the heating is generated. Figure 7b and c show two such images, extracted from the marked pixel columns *A* and *B* in Figure 7a. It is possible to evaluate these temperature images, but as it is mentioned at the beginning of this section, such IR images can be affected by inhomogeneous emissivity values, which further could cause false or missing defect detection. In order to be able to apply also for such an IR sequence the Fourier transform, first the images have to be shifted to the same position. As it is visible in Figure 7b and c the object is depicted on different positions. If the speed of the motion is selected in a way that between recordings of two consecutive images ($t_{camera} = 1/f_{camera}$) the object moves one or multiple number of pixels ($s = n_{pixel}$), then this means a re-ordering of the pixels and just shifting the object in all the images to the same position. For this quasi-static IR sequence, the Fourier transform can be applied with the same advantages as for the static measurement [25].

If during t_{camera} the object moves with a speed which does not correspond to a shifting of a multiple integer number of pixels, then an interpolation between the images is required for shifting the objects to the same position.

This re-ordering of the scanning measurement requires a constant motion speed. This speed can be either measured or eventually extracted from the IR images themselves.

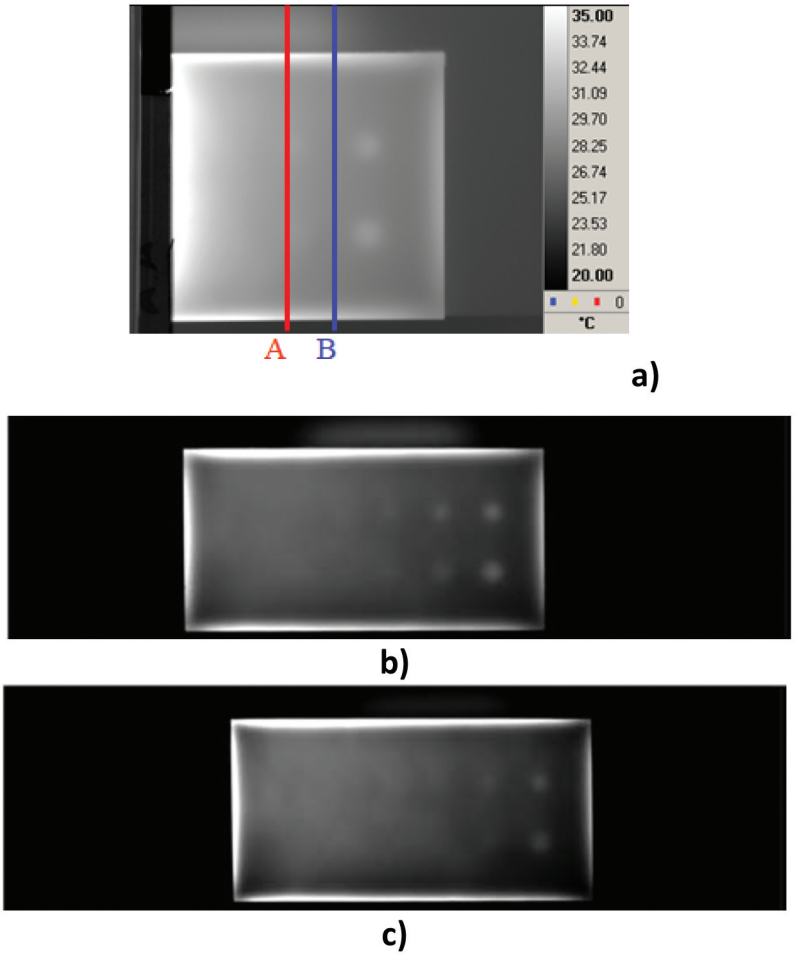

Figure 7. IR image of a scanning measurement with markings of two pixel columns (a); IR image reconstructed from the column 'A' (b); IR image reconstructed from the column 'B' (c).

Such an extraction requires an image registration, which finds the shifting between two images. Unfortunately, in many cases in IR images there is not enough contrast for a reliable registration. Therefore, in Ref [37] an additional calibration object with AprilTags [38] is suggested, which is recorded together with the inspected object. The AprilTags contain enough contrast for such a registration procedure. In Ref [37] it has been shown, that this kind of calibration object can be even used for scanning measurements, where the scanning speed is not constant, but always changing, as e.g. it is the case by a manual shifting of the object during the inspection.

5. Automatic defect detection

In order to achieve a fully automated inspection, the defects have to be located automatically in the images. In recent years, several different techniques have been developed and published, based on the complexity of the inductive thermography images, from

conventional image processing up to pattern recognition with shallow or with deep neural networks.

If the images have a strong signal-to-noise ratio, then it is possible to locate the lines of the surface cracks by applying image processing techniques, as e.g. edge detection technique. This technique can be used either on temperature images [39] or on phase images [40]. Figure 8 shows such an example, where railway rail was inspected using inductive thermography and the defects are very well visible and could be automatically located.

In other cases, when the cracks are rather short then, instead of detecting the crack lines, pattern recognition techniques are required. These techniques can be also used to distinguish between real defects and artefacts caused, e.g. be the geometry of the piece to be inspected. Castings and forgings have a complex geometry with several edges. In such a case, not only the defects but also the edges become warmer due to the inductive heating and the heat accumulation. Ref [41] shows an example of how the defects can be detected and separated from artefacts by shallow neural networks. In a first step, all the hot patches are segmented and then several features such as temperature increase, compactness, concavity have been extracted and used to train a neural network (NN). This NN is able then to classify whether the patch is caused by a crack or by the geometrical edge of the casting, see Figure 9.

In the recent years, various deep learning techniques have been developed for image evaluation and classification. Some of these methods have been applied to defect detection in different thermographic inspection techniques. As this paper focuses on the

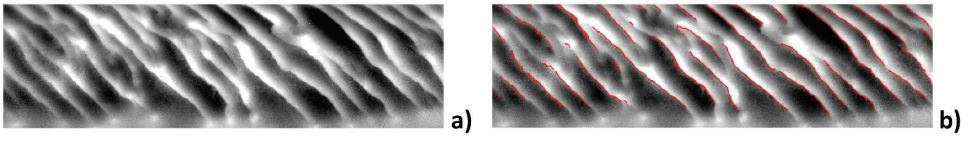

Figure 8. Phase image of a rail head with rolling contact fatigue cracks (a), the recognised crack lines are marked by red lines (b) [40].

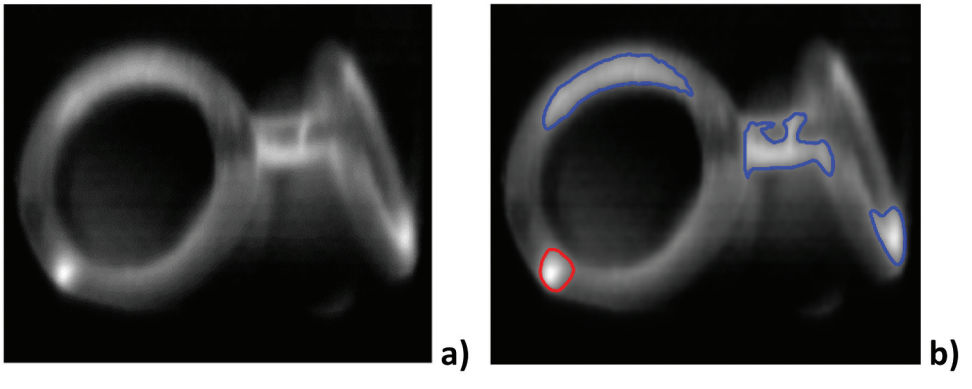

Figure 9. Temperature image of a casting after short inductive heating pulse(a); four warm patches have been identified, one of them was classified by the trained NN as a crack (red line) and three of them as artefacts, caused by edges (b) [41].

detection of surface cracks by inductive thermography, here are few examples for such applications, using deep learning techniques that have been proposed especially for inductive thermography.

Autoencoder can be used to extract relevant features of images. In Ref [42], defects at the backside of a sample are detected by using inductive thermography. In order to improve the images, an autoencoder has been trained to extract the underlying features and to construct new clearer images.

Deep learning algorithms need many images for supervised training to achieve proper generalisation and to avoid the so-called overfitting problem, where the method can only detect the defects, which were used for the training. Additionally, it is important that not all the samples are involved in the training, but several of them are used only in the testing and in the evaluation procedure. Different methods have been suggested how enough training images could be provided. In the case of transfer learning a pre-trained network is used, and this will be modified by teaching with additional images for special applications. The advantage is that for this transfer learning, much less images are required. The authors of Ref [43] show such an example: for detecting surface cracks in welding the temperature images after a short inductive heating pulse was used. As the crack lines have higher temperature than the surrounding surface, a transfer learning was proposed based on public data bases for retinal vessel images.

If there are enough defective samples with known defects, then these can be used for the training of the network. The authors of Ref [44] used a U-net, a kind of convolutional neural network (CNN), to detect surface cracks in forgings. The parts were inspected by inductive thermography, and the phase images were evaluated by the network. Half of the 44 parts were used to train the U-net, and the other parts to evaluate the network performance by intersection over union (IoU) metric.

The largest weakness of deep neural networks, how to provide enough independent examples for the training, covering all the defects, which have to be then recognised by the trained network. Additional to real samples, simulation data can be used to this purpose as well. In Ref [45], phase images of inductive thermography results on welds in nickel-based superalloy are used to locate the defective areas around the cracks. For the training of a CNN, simulation data with additional noise was used. Afterwards, this trained network was used for semantic segmentation of the experimental results of real welded samples, in order to localise the defective regions. Figure 10 shows such an example, where first the image is segmented, as the network recognises the patterns around the short cracks. In the next step, these regions are enlarged and then inside the bounding polygons the crack length, the phase minima and maxima are determined. These values are then used for characterising each crack, one-by-one.

The authors of Ref [46] suggest additionally to defect location with a U-net, also an anomaly detection as a pre-processing step. The inductive thermography inspection was carried out on connecting rods of piston engines. For the training of the anomaly detection only non-defective images are necessary, which are more easily available than images with defects. A pre-trained CNN was used to learn, how images without defects look like. In the evaluation phase the network analyses the distance in the feature space for the images, to locate anomalies. This pre-processing step helps to detect possible defects, but in the following step then a U-net is used to locate the cracks with higher reliability.

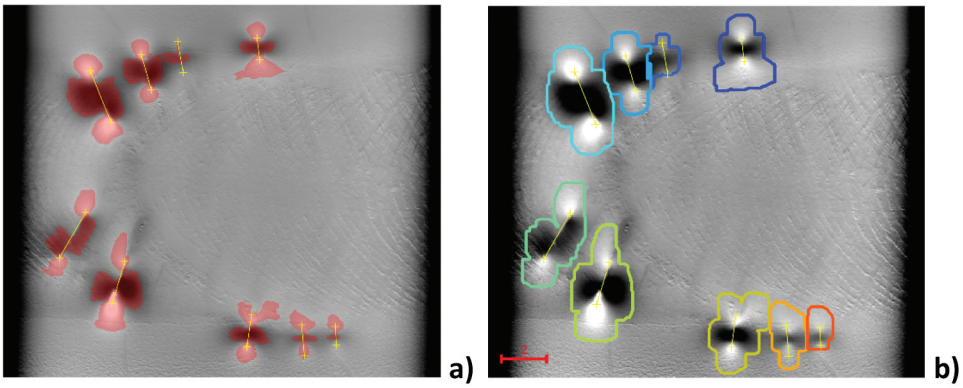

Figure 10. Semantic segmentation of a sample with nine surface crack regions (a); marking with contour lines around the crack regions (b).

In Ref [47], the authors suggest a further possibility on how to generate training images. A Generative Adversarial Network (GAN) is proposed, first to learn the characteristic features of defects from real measurements and then based on these to generate additional artificial images, which are then used for the supervised training. In Ref [47] it is also investigated how the probability of detection (POD) of surface cracks is affected, if: (a) only FEM results with additional noise are used for training; (b) the images are created by GAN and these images are used for training. The authors show, that the best detectability can be achieved, if both types of images, simulations and GAN generated images based on real measurements, are combined and used together for the training. Furthermore, also the performance of different deep learning structures, as e.g. YOLO and U-Net are compared in Ref [47].

6. Combination with other techniques

Several papers propose combining different NDT inspection techniques with inductive thermography, in order to obtain more information about the surface cracks. e.g. in Ref [48]. inductive thermography was combined with magnetic flux leakage inspection, and in Ref [49], it was fused with ultrasound testing to enhance the detectability.

IR images show the temperature distribution of the surface, but many details of the object are not visible, if they have the same temperature. This sometimes makes it difficult to interpret the IR images. It is therefore a great advantage to use a visible camera in addition to the IR camera and to fuse the images from both. For different applications several techniques have been proposed. In the case of traditional image fusion, first the relevant features are extracted from both image types to register the images to each other and this information is used then in the fusion procedure. Other new approaches use different deep neural networks, as e.g. CNN and GAN, to catch the information which are then used for the fusion. For a more detailed description the interested user is referred to extensive review papers, as e.g. Refs [50] and [51]. In many cases it is helpful, if just the object edges localised in the visual images, are shown in the IR images [52]. Also, in the case of inductive thermography, it helps to

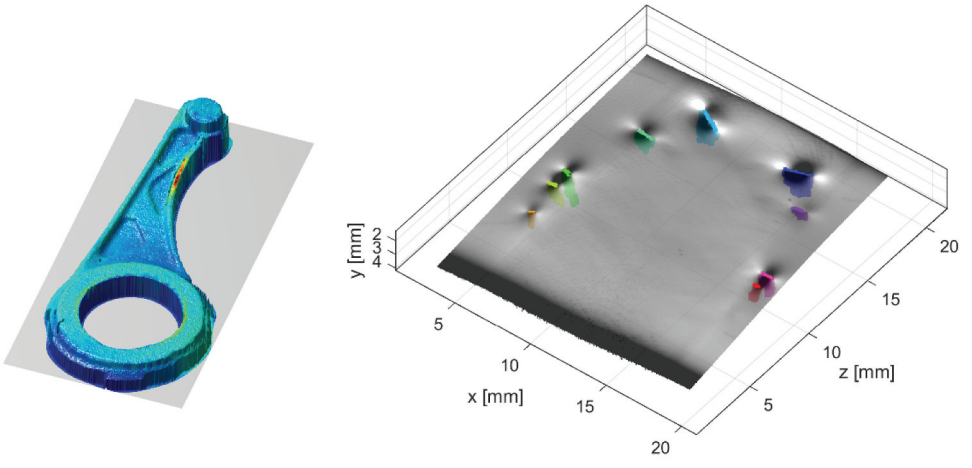

Figure 11. 3D surface of a level measured by light-sectioning and combined with thermographic results, revealing a surface crack by higher temperature (a); CT result of a sample with the detected surface cracks marked with different colours, combined with the inductive thermography phase image of the sample (b).

interpret the IR results, by combining the images from both types of cameras. It is very helpful in locating the defects on the real work-piece, after they have been detected in the IR image [53].

The 3D geometry of a work-piece can be measured, e.g. by using the light sectioning technique, which can be then combined with inductive thermography results. In Ref [54], the 3D surface data of the level and its IR image obtained with inductive thermography are registered to each other. This is performed based on geometrical features of the level, which can be located in both types of images. Then, the IR image is mapped onto the 3D surface, see the result in Figure 11a. This technique is very helpful in localising a defect on the sample, in this case, a forging lap along the right side of the level. An additional advantage is that artefacts, caused by strong edges of the sample, can be identified and filtered out due to the 3D information.

The real size, as depth and shape of the defects below the surface can be measured by computed tomography (CT). Combining such CT results with the inductive thermography results can be used to see what kind of phase patterns the different cracks produce [55], see e.g Figure 11b. It can also be in this figure recognised that around deeper defects a larger phase contrast occurs.

7. Probability of detection

For industrial applications, it is very important to know the reliability of an inspection technique. The probability of detection (POD) is a usual technique to give a measure for this reliability. The two mostly used techniques for POD calculations are the hit/miss [56] and the '*â versus a*' [57] technique. In the hit/miss method only regarded, whether a defect is detected (hit) or not detected (missed). In the case of '*â versus a*' a signal *â* is

determined, which is a kind of function of the defect size *a*. Based on a decision threshold it is then decided, whether the current indication is a defect or not.

The POD depends on all kind of parameters:

- Material: in ferritic materials it is much easier to detect cracks, as the inductive heating is more efficient, than in non-magnetic metal;
- Experimental setup: as e.g. what kind of IR camera with what kind of optic is used and what kind of inductive heating is applied.
- Evaluation technique: whether single temperature images are used for the defect detection or evaluation techniques, as e.g. Fourier transform has been applied and the cracks should be detected in the phase images.

In Ref [58], the POD of small, sub-millimetre fatigue cracks in three different metals (ferritic-steel, nickel-based superalloy and titanium) using inductive thermography was investigated. The temperature images at the end of the heating pulse with 50 ms duration were used for the POD calculations. The results show that $a_{90/95}$ (crack length having 90% POD with 95% confidence) is 0.60 mm for ferritic steel, 0.78 mm for titanium and 1.50 mm for the nickel-based superalloy.

For POD calculations many parts with known defects are necessary. These can be manufactured artificially, or collected from real defective samples. An additional possibility is to use finite element simulations for a model-assisted POD calculation, as e.g. it has been done in Ref [59]. In this paper POD calculations for small surface cracks in Inconel 718 (nickel-based superalloy) were carried out based on phase images, combining experimental results with FEM simulations. It is also shown that the POD does not depend only on the length of the crack, but also on its depth, which therefore requires a 2-dimensional detection function. In Ref [60], both POD techniques of hit/miss and the '*â versus a*' are compared for the same cases as in Ref [59], with the result that in Inconel 718 $a_{90/95}$ is in the range 0.8–0.9 mm, which proves an excellent detectability for surface defects.

The POD depends also whether the defect detection is made by a human expert or by a fully automated software. In Ref [47], it is investigated what is the $a_{90/95}$ value, if the defect should be located by a deep neural network. It has been found that the network has a slightly higher $a_{90/95}$ value, in the range of 0.94 mm and 1.14 mm, showing that a human expert can still better recognise defects than the software, on the other hand, with all the known drawbacks of human decisions.

Industrial applications

Traditionally, for inline non-destructive testing for surface crack detection, one of two inspection techniques is used: magnetic particle inspection for ferromagnetic materials or liquid penetrant inspection for non-magnetic materials. Both of these techniques are usually performed manually by humans, both do not provide information on depth of the crack in the sample and both require several chemicals that are not environmentally friendly. Inductive thermography has great potential to replace these two methods in industrial applications.

In the early 1980s, a commercial inspection system, called Therm-O-Matic, was offered and extensively used in the industry for detecting surface cracks in steel bars and billets

[61]. The long steel billets were moved through an induction coil at a speed of approximately 1 m/s and four line scan IR cameras recorded the temperature at the four sides of the billet behind the induction coil. These temperature profiles were analysed to locate surface cracks. To reduce the inhomogeneous emissivity of the surface, the specimen was moistened with water prior to inductive heating. This system has been developed further first by Corus Research [62] and then by Foerster [63], using FPA IR cameras instead of line scan cameras. Based on the recording of the 2D IR images, the temporal change of the temperature can be analysed. This improves the defect detectability and reduces false detection.

Induction thermography is an excellent method for inspecting welds. This can be done in a two-sided mode, where the IR camera and the induction coil are placed on different sides of the weld, and the heat flow through the weld is analysed to locate and characterise different defect types, as e.g. local cavities or 'false friends' [64]. In Ref [65], the authors compares the inspection results obtained by inductive thermography with radiographic and with dye penetrating results, as these two methods are currently the state of the art techniques, and usually used in the industry. This comparison is performed for real and for artificial irregularities, proving the excellent capabilities of the thermographic inspection.

If the weld is only accessible from one side, then inductive thermography can be used to detect surface cracks in the welds. The authors of the Refs [66] and [67] generated with the so-called Varestraint test machine realistic small cracks in the weld of Inconel 718 samples, by applying pressure during the welding process. These samples are similar, as shown in Figures 5 and 6. The welds were inspected by inductive thermography. For a fully automated inspection the inductor is positioned along the weld by a robot, and the phase images are used for automatic evaluation of the inspection. POD calculation shows that $a_{90/95}$ is around 0.8–0.9 mm, which means cracks with this length have a 90% POD with 95% confidence [47,60].

There are several norms, how welds have to be NDT inspected. For thermographic inspection of welds there is until now just a German standard available, see Ref [68].

Forgings and castings, produced specifically for the aeronautic and for the automotive industry must be 100% inspected for possible defects. Parts, as generator components, compressor blades, or other aircraft engine components have high safety requirements. As these parts often have complex geometries, manual inspection by humans using magnetic particle inspection or fluorescent penetrant inspection is applied. However, inductive thermography has been shown to have great potential here, due to its ability to be highly automated and to provide information on the depth of surface cracks. The authors of the paper [69] presents automated inductive thermography testing of rotor wedges. The parts are moved through a double inductor with 45° to the motion direction, and in this way cracks in all directions can be located. In Ref [70], a fully automated testing of compressor blades for an aircraft engine is published. A robot places the blade to the induction coil, and during the short heating pulse the infrared image sequence is recorded and evaluated to a phase image. This is then automatically analysed to locate cracks. In Ref [71], the authors inspected aircraft engine components, as an engine disc to detect fatigue cracks, where the complex geometry of the part means a challenge for the inspection. In Refs [72,73] and [46], different forged parts with complex geometry, as e.g. artificial hip joints, wheel hubs, car ball joint, were inspected by inductive thermography

and the results compared to the traditional NDT methods as magnetic particle and liquid penetrant testing. As it has been shown in the previous section, for the automated detection of cracks deep neural networks have been developed [46]. In Ref [19], a fully automated inspection of castings is proposed, where a robot handles the pieces positioning them with high reproducibility. The images of the inspected parts are compared with images of reference parts, and in this way artefacts caused by edges and corners of the parts are filtered out and not marked as defects. In Refs [2,10] and [74], the authors give different examples of how inductive thermography can be used in industrial applications for crack detection. Results are shown for different forged parts, for gear tooth, and also for inspection of a rail.

Railway inspection is another very important area. Nowadays rails are typically inspected using eddy current testing for surface cracks, and ultrasonic testing for volumetric defects. Inductive thermography also has a great potential in this area, as several papers published in the recent years have shown [39,40,75–79]. Typical defects, such as rolling contact fatigue (RCF) cracks or squats must be localised at an early stage, before highly dangerous accidents may occur. The inspection is performed by moving a test car and scanning the rail surface with inductive heating. The main challenge in this case is the speed, as a high speed of movement requires a high recording speed of an IR camera and a fast evaluation of the images.

For industrial applications, it is important to have a standard for the inspection. In Germany there is already a standard available for inductive thermography since 2018 [80]. The standard shortly summarises the principle of the inductive thermography, describing which defects in which material can be detected and which ones not, using this inspection technique. Then, the induction generator and inductor requirements are handled. The specifications and requirements for IR cameras are listed in the standard, as well. The evaluation techniques are just shortly mentioned in this standard, as they are described in more detail in another standard [81]. The standard gives also suggestions for different categories of reference test specimens [82]:

- Type 1 reference specimens are for controlling the calibration of the inspection system;
- Type 2 reference specimens should have artificial defects in order to prove the defect detectability in different materials, as e.g. defects with different depth, with different length, different crack entry angles, and reference specimens with artificial defects in different distances to each other, in order to prove the spatial resolution of the technique;
- Type 3 reference specimens are real samples with usual defects, which means scraps collected during the production.

This German standard [80] will soon be also available in Europe through the work of the European Committee for Standardization (CEN).

Summary and outlook

Inductive thermography has been greatly improved over the last few decades, and it will be increasingly used also in the industry. The method is non-contact, fast,

and it can be fully automated, which are very important factors for its future usage. As it does not require usage of chemicals, as the currently applied techniques of magnetic particle and liquid penetrant testing, it has a high opportunity to replace these two methods in the future. Furthermore, the inductive thermography contrast caused by a crack depends on its depth, which allows also a depth estimation additionally to the crack localisation. This is an additional argument for the usage of inductive thermography, as both traditional techniques do not provide this crack characterisation possibility. In other cases, where very high reliability is required, inductive thermography can be used as an additional tool to the traditional techniques, and with the fusion of the different techniques to achieve an even higher detectability.

The development of new different inductors, from water-cooled copper coils with different geometries to air-cooled inductors with ferrite cores, allows the technique to be scaled and adapted to all kind of tasks. New developments of smaller and smaller generators will make it possible to have portable inductive thermography inspection equipment. IR cameras have also improved greatly in the recent years, with better temperature and spatial resolution, with higher recording frequency and with smaller sizes. As also the prices of the IR cameras are decreasing, this helps in the dissemination of the thermographic inspection technique.

The rapid development of image processing methods supported by machine learning techniques offers the possibility of fully automated defect detection. The big question is, how to collect all the images, which are necessary for the training of the deep networks. These images can be taken from inspection of artificial defects, but they have usually larger opening than real cracks with µm openings, therefore artificial cracks are closer to notches than to real defects. The training images can be collected from scrap parts, but as usually not many defective parts are produced, this way is also not easy. However, the combination of these measurement result with simulations, and artificially generated defect images by GAN technique, can deliver enough training data. But for a fully automated detection of all kind of defects, all possible defects have to be covered by the training data set, which can be a large challenge.

These trends are opening up more and more opportunities for industrial applications for this inspection technique, and the possibility of replacing the traditional NDT techniques as magnetic particle or liquid penetrant inspection by a fully automated inductive thermography, from handling of the work-pieces up to defect localisation and defect characterisation.

Disclosure statement

No potential conflict of interest was reported by the author(s).

ORCID

Beate Oswald-Tranta http://orcid.org/0000-0002-1994-3039

References

[1] Maldague X. Nondestructive testing handbook: vol. 4, thermal and infrared testing (IR). 4th ed. Columbus (OH): American Society for Nondestructive Testing (ASNT); 2024, Chapter 11, Part 8, 2024.

[2] Netzelmann U, Walle G, Lugin S, et al. Induction thermography: principle, applications and first steps towards standardisation. QIRT J. 2016;13(2):170–181. doi: 10.1080/17686733.2016.1145842

[3] Kidangan RT, Krishnamurthy CV, Balasubramaniam K. Identification of the fiber breakage orientation in carbon fiber reinforced polymer composites using induction thermography. NDT & E Int. 2021;122:102498. doi: 10.1016/j.ndteint.2021.102498

[4] Kidangan RT, Unnikrishnakurup S, Krishnamurthy CV, et al. Induction thermography for unidirectional CFRP composites: a novel inspection approach through global current path integration. Composite Struct. 2024;327:117678. doi: 10.1016/j.compstruct.2023.117678

[5] Guo J, Gao X, Toma E, et al. Anisotropy in carbon fiber reinforced polymer (CFRP) and its effect on induction thermography. NDT & E Int. 2017;91:1–8. doi: 10.1016/j.ndteint.2017.05.004

[6] Oswald-Tranta B, Tuschl C, Schledjewski R. Flash and inductive thermography for CFRP inspection. In: Proceedings of SPIE, Thermosense; Baltimore, Maryland, United States. XLI, 2019. Vol. 11004.

[7] Kidangan RT, Unnikrishnakurup S, Krishnamurthy CV, et al. Uncovering the hidden structure: a study on the feasibility of induction thermography for fiber orientation analysis in CFRP composites using 2D-FFT. Compos Part B: Eng. 2024;269:111107. doi: 10.1016/j.compositesb.2023.111107

[8] Oswald-Tranta B, Shepard SM. Comparison of pulse phase and thermographic signal reconstruction processing methods. In: Proceedings of SPIE Thermosense XXXV; Baltimore, Maryland, United States; 2013. Vol. 8705.

[9] Wang Z, Zhu J, Tian G, et al. Comparative analysis of eddy current pulsed thermography and long pulse thermography for damage detection in metals and composites. NDT & E Int. 2019;107:102155.

[10] Netzelmann U. Induction thermography of surface defects. In: Handbook of advanced nondestructive evaluation. Springer International Publishing, Cham; 2019. p. 1497–1522. doi: 10.1007/978-3-319-26553-7

[11] Oswald-Tranta B. Surface crack detection in different materials with inductive thermography. In: Proceedings of SPIE Thermosense XXXIX; Anaheim, CA, United States; 2017. Vol. 10214.

[12] Vrana J, Goldammer M. Defect detection mechanisms with induction and conduction thermography: current flow and defect-specific warming. QIRT J. 2020;17(2). doi: 10.1080/17686733.2019.1635350

[13] Wilson J, Tian GY, Abidin IZ, et al. Modeling and evaluation of eddy current stimulated thermography. J Nondestr Test Eval. 2010;25(3):205–218. doi: 10.1080/10589750903242533

[14] Oswald-Tranta B. Induction thermography for surface crack detection and depth determination. Appl Sci (Switz). 2018;8(2):257. doi: 10.3390/app8020257

[15] Oswald-Tranta B. Thermo-inductive crack detection. J Nondestr Test Evaluation. 2007;22(2–3):137–153. doi: 10.1080/10589750701448225

[16] Oswald-Tranta B. Detection and characterisation of short fatigue cracks by inductive thermography. QIRT J. 2021;19(4):239–260. doi: 10.1080/17686733.2021.1953226

[17] Oswald-Tranta B, Sorger M. Localizing surface cracks with inductive thermographical inspection: from measurement to image processing. QIRT J. 2011;8(2):149–164. doi: 10.3166/qirt.8.149-164

[18] IFF GmbH. Available online https://www.iff-gmbh.de/en/induction-technology/generatoren/, (accessed on Mai 2024).

[19] Oswald-Tranta B. Automated surface crack detection with inductive thermography. In: Proceedings of of the 20th World Conference on Non-Destructive Testing (WCNDT 2024); 2024 in Incheon, South Korea, e-Journal of Nondestructive Testing. p. 27–31. doi: 10.58286/30301

[20] De Vanna D, D'Accardi E, Dell'avvocato G, et al. Induction thermography: influence of testing parameters for different crack geometry. In: Society for Experimental Mechanics Annual Conference and Exposition; Cham. Springer Nature Switzerland; 2023. p. 73–82.
[21] Tang B, Hou D, Hong T, et al. Influence of the external magnetic field on crack detection in pulsed eddy current thermography. Insight. 2018;60(5):240–246. doi: 10.1784/insi.2018.60.5.240
[22] Urtasun B, Andonegui I, Gorostegui-Colinas E. Phase-shifted imaging on multi-directional induction thermography. Sci Rep. 2023;13(1):17540. doi: 10.1038/s41598-023-44363-5
[23] Lugin S, Müller D, Finckbohner M, et al. Automated surface defect detection in forged parts by inductively excited thermography and magnetic particle inspection". QIRT J. 2023:1–13. doi: 10.1080/17686733.2023.2266901
[24] DIN 54187. 2024–02 - entwurf, "non-destructive testing - active thermography with relative motion", DIN 54187 https://www.din.de (accessed on Oct 2024).
[25] Oswald-Tranta B, Sorger M. Scanning pulse phase thermography with line heating. QIRT J. 2012;9(2):103–122. doi: 10.1080/17686733.2012.714967
[26] Rogalski A. Infrared detectors. 2nd ed. Boca Raton, FL: CRC Press, Taylor and Francis Group; 2010.
[27] Oswald-Tranta B. Temperature reconstruction of infrared images with motion deblurring. J Sensors Sens Syst. 2018;7(1):13–20. doi: 10.5194/jsss-7-13-2018
[28] Maldague X, Marinetti S. Pulse phase infrared thermography. J Appl Phys. 1996;79(5):2694–2698. doi: 10.1063/1.362662
[29] Oswald-Tranta B. Time-resolved evaluation of inductive pulse heating measurements. QIRT J. 2009;6(1):3–19. doi: 10.3166/qirt.6.3-19
[30] Wu D, Busse G. Lock-in thermography for nondestructive evaluation of materials. Revue Générale de Thermique. 1998;37(8):693–703. doi: 10.1016/S0035-3159(98)80047-0
[31] Maierhofer C, Myrach P, Krankenhagen R, et al. Detection and characterization of defects in isotropic and anisotropic structures using lockin thermography. J Imag. 2015;1(1):220–248. doi: 10.3390/jimaging1010220
[32] Meola C, Carlomagno GM, Squillace A, et al. Non-destructive evaluation of aerospace materials with lock-in thermography. Eng Fail Anal. 2006;13(3):380–388.
[33] Sakagami T, Kubo S. Applications of pulse heating thermography and lock-in thermography to quantitative nondestructive evaluations. Infrared Phys Technol. 2002;43(3–5):211–218. doi: 10.1016/S1350-4495(02)00141-X
[34] Breitenstein O, Langenkamp M. Lock-in thermography". In: Itoh K, Lee T, Sakurai T, Sansen W Schmitt-Landsiedel D, editors. Springer series in advanced microelectronics. Berlin Heidelberg: Springer Verlag; 2003. p. 29–32.
[35] Riegert G, Zweschper T, Busse G. Lockin thermography with eddy current excitation. QIRT J. 2004;1(1):21–32. doi: 10.3166/qirt.1.21-32
[36] Oswald-Tranta B. Lock-in inductive thermography for surface crack detection in different metals. QIRT J. 2019;16(3–4):276–300. doi: 10.1080/17686733.2019.1592391
[37] Tuschl C, Oswald-Tranta B, Agathocleous T, et al. Scanning inductive pulse phase thermography with changing scanning speed for non-destructive testing. QIRT J. 2023. doi: 10.1080/17686733.2023.2170159
[38] Olson E. AprilTag: a robust and flexible visual fiducial system. In: IEEE International Conference on Robotics and Automation; Shanghai, China. IEEE; 2011. p. 3400–3407.
[39] D'Accardi E, Dell'avvocato G, Masciopinto G, et al. Evaluation of typical rail defects by induction thermography: experimental results and procedure for data analysis during high-speed laboratory testing. QIRT J. 2024:1–22. doi: 10.1080/17686733.2024.2340060
[40] Tuschl C, Oswald-Tranta B, Eck S. Inductive thermography as non-destructive testing for railway rails". Appl Sci. 2021;11(3):11, 1003. doi: 10.3390/app11031003
[41] Oswald-Tranta B, Sorger M, P O. Thermographic crack detection and failure classification. J Electron Imag. 2010 July-Sep;19(3):031204. doi: 10.1117/1.3455991

[42] Xie J, Xu C, Chen G, et al. Improving visibility of rear surface cracks during inductive thermography of metal plates using autoencoder. Infrared Phys Technol. 2018;91:233–242. doi: 10.1016/j.infrared.2018.04.016
[43] Moreno R, Gorostegui E, López de Uralde P, et al. Towards automatic crack detection by deep learning and active thermography. Chapter Book Adv Comput Intel. 2019:151–162. doi: 10.1007/978-3-030-20518-8_13
[44] Müller D, Netzelmann U, Valeske B. Defect shape detection and defect reconstruction in active thermography by means of two-dimensional convolutional neural network as well as spatiotemporal convolutional LSTM network. QIRT J. 2022;19(2):126–144. doi: 10.1080/17686733.2020.1810883
[45] Oswald-Tranta B, Lopez de Uralde Olavera P, Gorostegui-Colinas E, et al. Convolutional neural network for automated surface crack detection in inductive thermography. In: Proceedings of SPIE, Thermosense: Thermal Infrared Applications XLV; Orlando, (FL), USA; 2023 April May 30. Vol. 12536.
[46] Tout K, Samet N, Bouteille P. Automated defect detection on inductive thermography images using supervised and semi-supervised deep learning methods. e-J Nondestr Test. 2023 Sep;28(9). doi: 10.58286/28510
[47] Antero O, Muniategui A, Gorostegui-Colinas E, et al. Automatic detection based on deep learning of small cracks in induction thermography using images from FEM simulation models. In: Proceedings of 17th QIRT conference; Zagreb, Croatia; 2024.
[48] Gao Y, Tian GY, Li K, et al. Multiple cracks detection and visualization using magnetic flux leakage and eddy current pulsed thermography. Sensors Actuators A. 2015;234:269–281.
[49] Xiao X, Gao B, Tian GY, et al. Fusion model of inductive thermography and ultrasound for non-destructive testing. Infrared Phys Technol. 2019;101:162–170. doi: 10.1016/j.infrared.2019.06.016
[50] Ma W, Wang K, Li J, et al. Infrared and visible image fusion technology and application: a review. Sensors. 2023;23(2):599.
[51] Sun C, Zhang C, Xiong N. Infrared and visible image fusion techniques based on deep learning: a review. Electronics. 2020;9(12):2162. doi: 10.3390/electronics9122162
[52] Teledyne FLIR MSX. Available online https://www.flir.eu/discover/professional-tools/what-is-msx/, (accessed on Mai 2024).
[53] Tuschl C, Agathocleous T, Oswald-Tranta B, et al. Scanning inductive thermography using a μ-bolometer and a visual camera. In: Proceedings SPIE 12536, Thermosense: Thermal Infrared Applications XLV; 2023 June 12. Vol. 125360D. doi: 10.1117/12.2662819
[54] Oswald-Tranta B, P O. Fusion of geometric and thermographic data for automated defect detection. J Electron Imag. 2012;21(2):021108. doi: 10.1117/1.JEI.21.2.021108
[55] Oswald-Tranta B, Hackl A, Gorostegui-Colinas E, et al. Inspection of short surface cracks by inductive thermography and by computer tomography. In: Proceedings SPIE 13047, Thermosense: Thermal Infrared Applications XLVI; National Harbor, Maryland, United States; 2024.
[56] ASTM International. ASTM-E2862 -18 - standard practice for probability of detection analysis for Hit/Miss data, West Conshohocken, PA 19428–2959. United States: ASTM International; 2018.
[57] ASTM International. ASTM-E3023 - 15 - standard practice for probability of detection analysis for â versus a data. United States: ASTM International; 2015. West Conshohocken, PA 19428–2959.
[58] Weekes B, Almond DP, Cawley P, et al. Eddy-current induced thermography—probability of detection study of small fatigue cracks in steel, titanium and nickel-based superalloy. NDT E Int. 2012;49:47–56. doi: 10.1016/j.ndteint.2012.03.009
[59] Oswald-Tranta B, Hackl A, Lopez de Uralde Olavera P, et al. Calculating probability of detection of short surface cracks using inductive thermography. QIRT J. 2022;19(4):239–260. doi: 10.1080/17686733.2022.2152259
[60] Oswald-Tranta B, Lopez de Uralde Olavera P, Gorostegui-Colinas E, et al. Comparison of hit/miss and 'â versus a' POD calculations for short surface cracks using inductive thermography",

in proceedings of the European conference on non-destructive testing (ECNDT) from 3 to -7 of July 2023 in Lisbon, Portugal. Res Rev J Nondestr Test. 1(1). doi: 10.58286/28076

[61] Kremer KJ, Kaiser W, Möller P, et al. Das Therm-O-Matic-Verfahren - ein neuartiges Verfahren für die Online-prüfung von Stahlerzeugnissen auf Oberflächenfehler. Stahl u. Eisen. 1985;105:71–76. (in German).

[62] Wullink J, Darses P. On-line thermography applied to crack detection in steel billets. In: Proceedings of 5th QIRT conference; Reims, France; 2000. doi: 10.21611/qirt.2000.031.

[63] Koch S, Schroeder J. In-line inspection of hot-rolled steel billets by heat flux thermography. In: Proceedings of 11th QIRT conference; Neapel, Italy: QIRT conf; 2012.

[64] Srajbr C. Induction excited thermography in industrial applications. In: Proceedings of 19th WCNDT conf; Munich, Germany; 2016.

[65] Prints E, Kryukov I, Mund M, et al. Potential of active thermography as a non-destructive testing method for quality assurance of welded joints. 2nd European NDT & CM days. Prague, Czech Republic; 2021 Oct 4–7. Available from: https://www.ndt.net/?id=26437

[66] Gorostegui-Colinas E, Hidalgo-Gato R, de Uralde PL, et al. Induction thermography based inspection of EBW and TIG welded inconel 718 components: steps towards industrialization. In: Proceedings of SPIE 11409, Thermosense: Thermal Infrared Applications XLII; 2020 May 18. Vol. 114090D. doi: 10.1117/12.2558265

[67] Gorostegui-Colinas E, Muniategui A, de Uralde PL, et al. A novel automatic defect detection method for electron beam welded inconel 718 components using inductive thermography. In: Proceedings of 14th QIRT conf; Berlin, Germany; 2018.

[68] DIN 54186. 2022–09 non-destructive testing – testing of laser-beam welded joints using active thermography, Available online https://www.din.de (accessed on Mai 2024).

[69] Goldammer M, Mooshofer H, Rothenfusser M, et al. Automated induction thermography of generator components. In: AIP Conference Proceedings; 2010. Vol. 1211. p. 451–457, doi: 10.1063/1.3362428

[70] Zenzinger G, Bamberg J, Satzger W, et al. Thermographic crack detection by eddy current excitation. Nondestr Test Evaluation. 2007;22(2–3):2–3, 101–111. doi: 10.1080/10589750701447920

[71] Genest M, Li G. Inspection of aircraft engine components using induction thermography. In: IEEE Canadian Conference on Electrical & Computer Engineering (CCECE); (QC), QC, Canada; 2018. p. 1–4. doi: 10.1109/CCECE.2018.8447832

[72] Bouteille P, Legros G, Maillard S, et al. Induction active thermography as an alternative to magnetic particle inspection. In: Proceedings of 11th QIRT Conf; Naples, Italy; 2012.

[73] Bouteille P, Legros G. Induction thermography as an alternative to conventional NDT methods for forged parts. In: Proceedings of 12th QIRT conference; Bordeaux, France: QIRT Conf; 2014 doi: 10.21611/qirt.2014.134

[74] Netzelmann U, Walle G. Induction thermography as a tool for reliable detection of surface defects in forged components. In: Proceedings of 17th World Conference on Nondestructive Testing (WCNDT); Shanghai, China; 2008 Oct 25–28.

[75] Wilson J, Tian G, Mukriz I, et al. PEC thermography for imaging multiple cracks from rolling contact fatigue. NDT & E Int. 2011;44(6):505–512. doi: 10.1016/j.ndteint.2011.05.004

[76] Peng J, Tian GY, Wang L, et al. Investigation into eddy current pulsed thermography for rolling contact fatigue detection and characterization. NDT & E Int. 2015;74:72–80. doi: 10.1016/j.ndteint.2015.05.006

[77] Li H, Gao B, Lu X, et al. Dynamic rail near-surface inspection of multi-physical coupled electromagnetic and thermography sensing system. IEEE Trans Instrum Meas. 2023;72:1–13. doi: 10.1109/TIM.2022.3224531

[78] Tuschl C, Oswald-Tranta B, Eck S, et al. Scanning pulse phase thermography for surface defect detection in manganese steel turnout frogs". In: Proceedings of the European conference on non-destructive testing (ECNDT) from 3-7 of July 2023 in Lisbon, Portugal. Res Rev J Nondestr Test. 1(1). doi: 10.58286/28220

[79] Vaibhav T, Balasubramaniam K, Kidangan R, et al. Eddy current thermography for rail inspection. In: Proceedings of 13th QIRT Conference; Gdansk,Poland; 2016.

[80] DIN 54183:2018–02. Non-destructive testing-thermographic testing- eddy-current excited thermography, Available online https://www.din.de (accessed on Jan.2018).
[81] EN 17119:2018–10. Non-destructive testing - thermographic testing - active thermography, Available online https://www.din.de (accessed on Dec.2024).
[82] EN 16714–1:2016–11. Non-destructive testing - thermographic testing –part 1: General principles, Available online: https://www.din.de (accessed on Dec 2024).